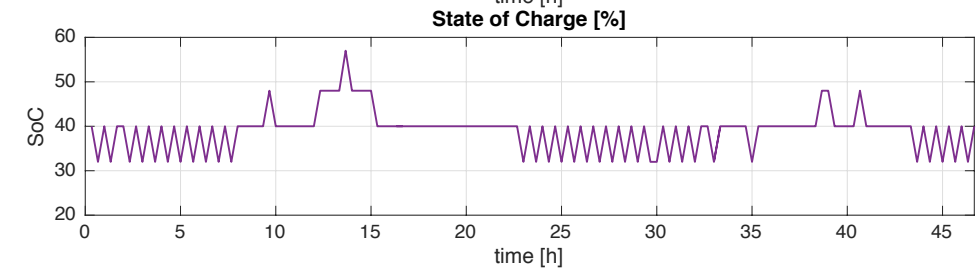
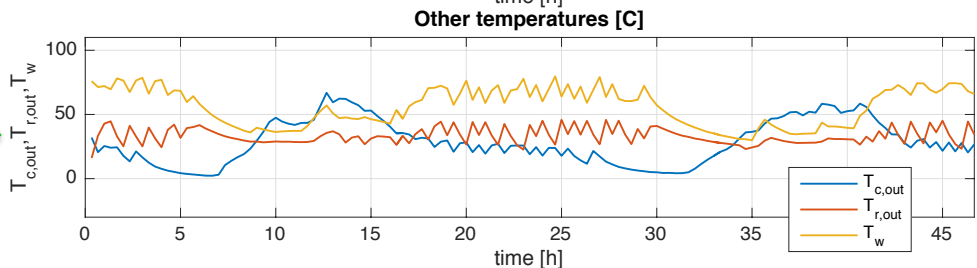
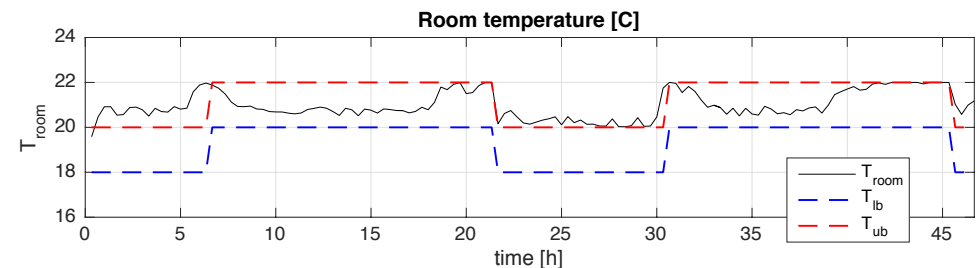




HYBRID MPC



Optimal energy management of a small-size building via hybrid model predictive control[☆]

Albina Khakimova^a, Aliya Kusatayeva^a, Akmaral Shamshimova^a, Dana Sharipova^a, Alberto Bemporad^b, Yakov Familiant^c, Almas Shintemirov^c, Viktor Ten^a, Matteo Rubagotti^{d,*}

^aNational Laboratory Astana, 53 Kabanbay Batyr Ave, Z05H0P9 Astana, Kazakhstan

^bIMT Institute for Advanced Studies, Piazza S. Ponziano 6, 55100 Lucca, Italy

^cNazarbayev University, 53 Kabanbay Batyr Ave 53, Z05H0P9 Astana, Kazakhstan

^dUniversity of Leicester, University Road, LE1 7RH Leicester, United Kingdom

Abstract

This paper presents the design of a Model Predictive Control (MPC) scheme to optimally manage the thermal and electrical sub-systems of a small-size building (“smart house”), with the objective of minimizing the expense for buying energy from the grid, while keeping the room temperature within given time-varying bounds. The system, for which an experimental prototype has been built, includes PV panels, solar collectors, a battery pack, an electrical heater in a thermal storage tank, and two pumps on the solar collector and radiator hydraulic circuits. The presence of binary control inputs together with continuous ones naturally leads to using a hybrid dynamical model, and the MPC controller solves a mixed-integer linear program at each sampling instant, relying on weather forecast data for ambient temperature and solar irradiance. The procedure for controller design is reported with focus on the specific application, and the proposed method is successfully tested on the experimental site.

Keywords: Model predictive control (MPC), Hybrid model predictive control (HMPC), Building control, Temperature control, Energy management systems.

1. Introduction

The use of various advanced control schemes, and in particular Model Predictive Control (MPC), has been recently proposed to improve the thermal efficiency of buildings beyond that obtainable with traditional methods [1, 2]. The general idea behind MPC for building control is to use a thermal model of a building and future temperature set points, possibly together with the forecast of weather and future energy prices, to predict the evolution of the system variables in real time. A control action is computed to minimize a cost function depending on the predictions, while satisfying given operational constraints. Even though the prediction typically spans over several hours, the control law is recomputed within short time intervals, typically from a few minutes to one hour.

In recent years, MPC has been employed for building heating and cooling systems, based on deterministic and stochastic models in, among others, [3–9] and [10–12], respectively. In some cases, a number of system variables are discrete in nature (e.g., some actuators can only be turned on/off), which requires the use of the so-called *hybrid MPC* approach [13–18]. In all the cited works, the aim is to provide a certain level of comfort to the occupants (e.g., for heating systems, impose lower bounds on room temperatures), while minimizing the energy consumption or the total cost of energy.

On the other hand, MPC is also increasingly used for the optimal schedule of energy sources in different application domains, such as hybrid electric vehicles [19, 20]. The use of MPC for overall energy management of buildings, where the thermal management is considered as one of many factors, has been analyzed, for instance, in [21]. One of the current trends is to use large-scale models of all the energy sources and the loads in buildings (including, for instance, charging of plug-in hybrid electric vehicles) in order to minimize the overall energy consumption [22–24].

In this paper, we propose a hybrid MPC control strategy applied to a prototype small-size building (referred to as “smart house” in the remainder of the paper) built inside the Nazarbayev University campus (Fig. 1). The goal is to keep the room temperature within given time-varying boundaries, at the same time managing the electrical and thermal storage, with the aim of minimizing the expense for buying electricity from the grid. Indeed, a building that draws less power from the grid contributes to reduce both the overall energy production from centralized power plants, and the load on the power distribution network, to which a continuously increasing number of residential and industrial consumers are being connected. This is particularly important in developing countries such as Kazakhstan, which are aiming at decreasing their dependence on fossil energy sources. In any realistic scenarios, it is important to evaluate the time needed for depreciation of the equipment in order to determine the advantages and/or disadvantages of the proposed solution. These will depend, among other factors, on the climate of the specific location, and on the prices of equip-

[☆]The first four authors contributed equally. The work was coordinated by M. Rubagotti, affiliated with Nazarbayev University during the preliminary part of the project activities.

*Corresponding author: M. Rubagotti. Email mr298@le.ac.uk, tel. +44-(0)116-233-1761, fax: +44-(0)116-252-2619.

ment and electricity from the grid. In turn, these factors depend on the specific country and geographic area where the building is situated, and on the energy policies of the country itself. All these considerations should be taken into account during the design of the smart house: in this paper, on the other hand, we consider how to optimize the system behavior in real-time, after the design process has been completed.

The energy-management approach presented in this paper requires first to obtain a control-oriented state-space dynamical model of the system, based on real data from the experimental site. The presence of binary control variables (pumps, electrical load powered from the grid or from the battery pack) makes the process a hybrid dynamical system. For this reason, the proposed MPC control law requires solving a mixed-integer optimization problem online. In particular, this consists of a mixed-integer linear program (MILP), formulated following the ideas proposed in [25].



Figure 1: (a) exterior of the smart house, including PV panels and solar collectors; (b) interior, including control computer, battery pack and charge controller; (c) interior, including thermal storage tank and pumps

The paper is structured as follows: Section 2 introduces the modeling of the smart house as a hybrid system, while Section 3 describes the design of the MPC controller. The experimental results and their discussion are presented in Section 4, and conclusions are drawn in Section 5.

The contribution of this paper consists of the proposal and experimental implementation of a strategy for the optimal management of batteries, renewable energy sources, and thermal storage elements at the same time, for a prototype small-size residential building. A preliminary version of the method pro-

posed in this paper can be found in [26], where an early version of the described control strategy was presented, and tested only in simulation.

Nomenclature

A, B_1, \dots, B_4	MLD model matrices
c_{cf}	cloud coefficient
c_1, \dots, c_{19}	model parameters
d, \hat{d}	measured/forecast vectors of uncontrolled inputs
E_e, \hat{E}_e	measured/forecast solar irradiance [W/m^2]
$\hat{E}_{e,cs}$	forecast clear-sky solar irradiance [W/m^2]
k	discrete time index
$J_{t,n}$	total electricity cost from time t for n sampling instants
i_{pv}	current generated by the PV array [A]
N	prediction horizon
P_a	power drawn by the appliances [W]
P_c	power drawn by the collector pump [W]
P_r	power drawn by the radiator pump [W]
P_{res}	power drawn by the auxiliary heater (resistor) [W]
P_{tot}	overall power consumption [W]
$P_{totgrid}$	power consumption from grid [W]
q_e	electricity price [KZT/kWh]
$q_{e,d}$	day electricity price [KZT/kWh]
$q_{e,n}$	night electricity price [KZT/kWh]
SoC	battery state of charge [%]
u_c	collector pump on/off control signal {0,1}
u_{grid}	transfer switch on/off control signal {0,1}
u_r	radiator pump on/off control signal {0,1}
u_{res}	resistor control signal (duty cycle) [0,1]
T_{amb}, \hat{T}_{amb}	measured/forecast ambient temperature [$^{\circ}\text{C}$]
$T_{c,out}$	collector outlet temperature [$^{\circ}\text{C}$]
$T_{lb,k}$	lower bound on T_{room} at time k [$^{\circ}\text{C}$]
$T_{r,out}$	radiator outlet temperature [$^{\circ}\text{C}$]
$T_{ub,k}$	upper bound on T_{room} at time k [$^{\circ}\text{C}$]
T_w	temperature of the fluid in the tank [$^{\circ}\text{C}$]
T_{room}	room temperature [$^{\circ}\text{C}$]
T_s	sampling interval (= 20) [min]
u	vector of control variables
\mathbf{u}	MPC control sequence
\mathbf{u}^*	optimal MPC control sequence
\mathcal{U}	set of control constraints
x	vector of state variables

X_k set of state constraints at time k
 z vector of auxiliary variables
 α proportionality coefficient between E_e and i_{pv} [Am^2/W]
 β constant ($= 10^{-3}T_s/60$) [Am^2/W]

2. Hybrid modeling of the smart house

2.1. Description of the experimental facility

The prototype smart house (Figs. 1-2) is composed of two rooms, with a total volume of 84 m^3 . Walls, floor and roof are made of three-layer frameless sandwich-type wall panel, thermally insulated with basalt fiber (thickness: walls 100 mm, roof and floor 150 mm). A stack of lead-acid batteries (eight batteries Effekta BTL 12-200), charged by PV panels (14 solar modules Alfasolar Pyramid 60P/250), powers the electrical load. This consists of two pumps (on the hydraulic circuits of the solar collector and of the radiator, whose drawn power is referred to, respectively, as $P_c = P_r = 300 \text{ W}$) and an auxiliary heater (resistor) in a 200-litre thermal storage tank (drawn power $P_{res} = 2000 \text{ W}$). The pumps can be either switched on or off by the control system: $u_c \in \{0, 1\}$ determines whether the collector pump is on ($u_c = 1$) or off ($u_c = 0$), and similarly $u_r \in \{0, 1\}$ for the radiator pump. On the other hand, $u_{res} \in [0, 1]$ is a continuous variable representing the percentage of time in each sampling interval in which the resistor is powered (duty cycle): if $u_{res} = 0$ the coil is off, if $u_{res} = 1$ the coil is on full power, and all intermediate values are allowed. Although this variable is binary in nature, converting it to a continuous one by using a duty cycle simplifies the control problem as compared to the preliminary approach of [26]. In addition to pumps and resistor, the system behavior is influenced by the power P_a drawn by the appliances, which include the control computer. In the scenarios studied in this paper, it is assumed that the load demand of the appliances is constant over time, and precisely $P_a = 300 \text{ W}$. Considering a sampling interval $T_s = 20$ minutes in which the values of the control variables remain constant, the average overall power consumption P_{tot} [W] is obtained as

$$P_{tot} = P_c u_c + P_r u_r + P_{res} u_{res} + P_a. \quad (1)$$

The electrical connections are such that the battery pack has a total capacity $Q = 800 \text{ Ah}$ and a nominal voltage $V_b = 24 \text{ V}$, and the common PV-Battery DC-bus is connected to an inverter. The load can be powered directly from the electrical grid or from the inverter via a transfer switch in the inverter switchgear, whose behavior is described by the binary variable $u_{grid} \in \{0, 1\}$: when $u_{grid} = 0$ the energy to the load is supplied from the battery pack and/or the PV array, while when $u_{grid} = 1$ the load is connected to the grid. The model of the electrical subsystem required for MPC design aims at describing the dynamics of the battery state of charge SoC [%] (monitored by the charge controller Power Tarom Steca 2070SC).

Although most electrical components (PV panels, batteries, and power converters) are nonlinear in nature, at a given operating mode and under standard assumptions, a linear model can represent an approximation of the actual behavior sufficient for control design: indeed, the proposed hybrid MPC control law will require a dynamical model including only linear or on/off components. The following conditions, already formulated in [26], are assumed: (a) the discharge power capability of the battery pack is much greater than the maximum output power of the PV array (implying that the voltage of the DC bus is imposed by the state of charge of the battery pack); (b) the useful energy (i.e., total energy \times depth of discharge) can be extracted from the battery pack in an interval of state of charge values for which the terminal voltage of the battery pack can be approximated as constant. Thus, the battery voltage can be approximated as constant for any rate of discharge if the state of charge does not become too low. Under these assumptions, the output current i_{pv} [A] generated by the PV array is approximately linearly proportional, by a constant α , to the solar irradiance E_e [W/m^2] for a constant voltage at the PV terminals, as confirmed observing the V-I curves in the data sheet of the PV array [27]. In order to find the value of α , the value of i_{pv} generated by the PV array has been measured, together with the solar irradiance E_e during normal operation of the system. As a result, by linear regression we obtained the relation

$$i_{pv} = \alpha E_e, \quad \alpha = 0.1218 \text{ Am}^2/\text{W}. \quad (2)$$

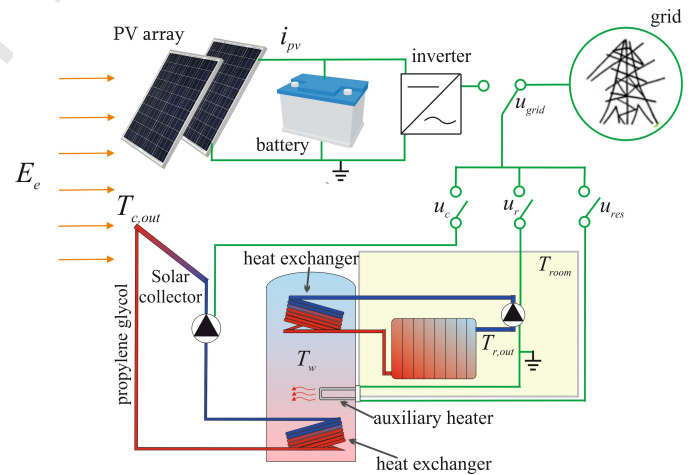


Figure 2: Schematic diagram of the smart house system

The storage tank can be heated by either the auxiliary heater or the solar vacuum collector, consisting of 20 vacuum heating tubes filled with propylene glycol. In order to obtain a lumped-parameters model useful for control design, the temperature of the evacuated tubes is defined as the average of $T_{c,out}$ and $T_{c,in}$, which are the outlet and inlet temperatures, respectively, of the solar collector. The heat capacity of the heating elements inside the thermal tank has been observed to be much smaller than that of the fluid flowing inside them: thus, it is assumed that all power supplied to the heating elements of the heat exchangers

goes directly into the fluid in the tank with no delay. Furthermore, the fluid inside the tank is assumed to have a uniform temperature T_w . The temperature of the fluid inside the radiator is defined as the average of $T_{r,out}$ and $T_{r,in}$ (i.e., the outlet and inlet temperature of the radiator, respectively), and we assume that no heat losses occur in the pipes connecting the tank with the radiator. In order to obtain an approximated model, simple enough for control design, the thermal subsystem was modeled by the four state variables $T_{c,out}$, $T_{r,out}$, T_w , T_{room} , the latter being the room temperature, assumed uniform. All four state variables are measured by sensors of type PT1000RTD or NTC10K. The external factors influencing the thermal dynamics are solar irradiance E_e and ambient temperature T_{amb} , which are measured by a Davis Vantage Pro weather station.

Overall, the vectors of states, control inputs, and uncontrolled inputs (disturbances) of the smart-house model are, respectively,

$$x \triangleq [T_{room} \quad T_w \quad T_{c,out} \quad T_{r,out} \quad \text{SoC}]^T, \quad (3)$$

$$u \triangleq [u_{res} \quad u_c \quad u_r \quad u_{grid}]^T, \quad (4)$$

$$d \triangleq [E_e \quad T_{amb}]^T. \quad (5)$$

2.2. Control objective

The electricity price q_e [KZT/kWh]¹, although not influencing the physical variables directly, will be taken into account by the MPC controller to determine the expense. As two-rate tariffs are being considered for introduction in Kazakhstan, we take into account a realistic scenario in which

$$q_e = \begin{cases} q_{e,d} & \text{between 6 a.m. and 11 p.m.} \\ q_{e,n} & \text{between 11 p.m. and 6 a.m.} \end{cases} \quad (6)$$

where $q_{e,d} = 105$ KZT/kWh, while $q_{e,n} = 56$ KZT/kWh.

Given a sequence of electricity price values $q_e(k)$ (k being the discrete-time index) sampled with the previously-mentioned sampling time $T_s = 20$ minutes, and average power consumption $P_{tot}(k)$, we obtain the overall expense in KZT (which the proposed control law will aim at minimizing), for n sampling intervals starting at time t , as

$$J_{t,n} \triangleq \sum_{k=t}^{t+n-1} \beta P_{tot}(k) q_e(k) u_{grid}(k), \quad (7)$$

with $\beta = 10^{-3} T_s / 60$. Notice that (7) accounts for the fact that, during the time intervals when $u_{grid} = 0$, the operational expense is equal to zero. The use of a specific tariff does not limit the validity of the proposed approach, which can be applied to any time-varying electricity price that is known a priori. In fact, q_e will be considered by the MPC controller as an external input with known future evolution.

¹The Kazakhstani Tenge (KZT), is the currency of the Republic of Kazakhstan.

2.3. Mathematical model of the smart house dynamics

The discrete-time model of the smart house, in which v^+ represents the one-step update of a generic variable v , is

$$T_{room}^+ = c_1 T_{room} + c_2 T_w + c_3 T_{r,out} + c_4 T_{amb} + c_5 E_e \quad (8a)$$

$$T_w^+ = c_6 T_{room} + c_7 T_w + c_8 (u_c) T_{c,out} + c_9 (u_r) T_{r,out} + c_{10} u_{res} \quad (8b)$$

$$T_{c,out}^+ = c_{11} (u_c) T_w + c_{12} T_{c,out} + c_{13} T_{amb} + c_{14} E_e \quad (8c)$$

$$T_{r,out}^+ = c_{15} T_{room} + c_{16} (u_r) T_w + c_{17} T_{r,out} \quad (8d)$$

$$\text{SoC}^+ = \text{SoC} + c_{18} (P_{totgrid} - P_{tot}) + c_{19} E_e \quad (8e)$$

where c_i , $i = 1, \dots, 19$ are experimentally identified parameters. Recalling the definition of P_{tot} in (1),

$$P_{totgrid} = \begin{cases} P_{tot} & \text{if } u_{grid} = 1 \\ 0 & \text{if } u_{grid} = 0 \end{cases} \quad (9)$$

represents the amount of power drawn from the grid.

It is important to notice that a subset of the parameters of the thermal model changes depending on the pumps operation: each of these parameters can take two values, depending on either u_c or u_r . This is due to the fact that the heat transfer coefficients between the storage tank on one side, and the collector/radiator on the other, are higher when the circulation of the propylene glycol is enforced by the corresponding pump. All parameters have been determined experimentally via grey-box closed-loop system identification [28, Ch. 13], following the same procedure described in [26, Sec. II]. The term $P_{totgrid} - P_{tot}$ in (12a) can either be equal to $-P_{tot}$ (when $u_{grid} = 0$) or to zero (when $u_{grid} = 1$). Three different scenarios can occur for the battery: (a) $u_{grid} = 1$, for which the battery is charged by the PV panels; (b) $u_{grid} = 0$ and $c_{18} P_{tot} < c_{19} E_e$, in which case the power produced by the PV panels is partially used to satisfy the load demand, and partially to charge the battery; (c) $u_{grid} = 0$ and $c_{18} P_{tot} > c_{19} E_e$, meaning that the battery contributes to powering the load, and is therefore in discharge mode. Finally, notice that the term $c_{19} E_e$ implies the linearity given by $i_{pv} = \alpha E_e$, and the fact that the increment of SoC in one sampling interval is assumed to be linearly proportional to the average value of i_{pv} in that interval.

Hybrid systems such as (8) can be modeled by *Discrete Hybrid Automata* (DHA) [25]. This is a versatile modeling framework in which continuous dynamics are expressed through linear difference equations, while discrete dynamics are defined by finite-state machines. In order to obtain a model more suitable for the numerical computations required by the MPC controller, a DHA can be translated into a set of linear integer equalities and inequalities known as *Mixed Logical Dynamical* (MLD) systems. In order to obtain a description of (8) in MLD form, a vector of continuous auxiliary variables is defined as

$$z \in \mathbb{R} = [z_1 \quad z_2 \quad z_3 \quad z_4 \quad z_5]^T. \quad (10)$$

To capture the switched linear dynamics given by the parameters that change their values depending on u_c and u_r , the following auxiliary real variables are defined:

$$z_1 = \begin{cases} c_{8,1}T_{c,\text{out}} & \text{if } u_c = 1 \\ c_{8,0}T_{c,\text{out}} & \text{if } u_c = 0 \end{cases} \quad (11a)$$

$$z_2 = \begin{cases} c_{9,1}T_{r,\text{out}} & \text{if } u_r = 1 \\ c_{9,0}T_{r,\text{out}} & \text{if } u_r = 0 \end{cases} \quad (11b)$$

$$z_3 = \begin{cases} c_{11,1}T_w & \text{if } u_c = 1 \\ c_{11,0}T_w & \text{if } u_c = 0 \end{cases} \quad (11c)$$

$$z_4 = \begin{cases} c_{16,1}T_w & \text{if } u_r = 1 \\ c_{16,0}T_w & \text{if } u_r = 0 \end{cases} \quad (11d)$$

$$z_5 = P_{\text{totgrid}} \quad (11e)$$

where $c_{i,1}$ and $c_{i,0}$ are the two possible realizations of parameter c_i . Also, P_{totgrid} was already formulated in the correct form to be one of the components of z , namely z_5 .

Then, (8) can be re-written as follows:

$$T_{\text{room}}^+ = c_1T_{\text{room}} + c_2T_w + c_3T_{r,\text{out}} + c_4T_{\text{amb}} + c_5E_e \quad (12a)$$

$$T_w^+ = c_6T_{\text{room}} + c_7T_w + z_1 + z_2 + c_{10}u_{\text{res}} \quad (12b)$$

$$T_{c,\text{out}}^+ = z_3 + c_{12}T_{c,\text{out}} + c_{13}T_{\text{amb}} + c_{14}E_e \quad (12c)$$

$$T_{r,\text{out}}^+ = c_{15}T_{\text{room}} + z_4 + c_{17}T_{r,\text{out}} \quad (12d)$$

$$\text{SoC}^+ = \text{SoC} + c_{18}(z_5 - P_c u_c - P_r u_r - P_{\text{res}} u_{\text{res}} - P_a) + c_{19}E_e \quad (12e)$$

or, in a more compact form

$$x^+ = Ax + B_1 u + B_2 z + B_3 d + B_4 \quad (13)$$

where $A \in \mathbb{R}^{5 \times 5}$, $B_1 \in \mathbb{R}^{5 \times 4}$, $B_2 \in \mathbb{R}^{5 \times 5}$, $B_3 \in \mathbb{R}^{5 \times 2}$, and $B_4 \in \mathbb{R}^5$ are constant matrices. Given the current values of x , u , and d , the time-evolution of (13) is determined by finding z from (9) and (11), and then updating x^+ in (13). A general explanation of how to obtain the auxiliary variables and generate MLD models is described in [25]. For ease of notation, and to avoid an excessive use of technicalities in the description of the hybrid MPC formulation, we refer to the state evolution of system (13) simply as

$$x^+ = f(x, u, d) \quad (14)$$

in which the presence of the auxiliary variables is not explicitly shown.

3. Hybrid model predictive control design

The first ingredient to define the MPC controller is the model, obtained in Section 2. Then, we define the following sets of operational constraints:

$$u \in \mathcal{U} \Leftrightarrow \begin{cases} u_{\text{res}} \in [0, 1] \\ u_c, u_r, u_{\text{grid}} \in \{0, 1\} \end{cases} \quad (15)$$

$$x \in \mathcal{X}_k \Leftrightarrow \begin{cases} T_{\text{room}} \in [T_{lb,k}, T_{ub,k}] \\ T_w \in [-5^\circ\text{C}, 80^\circ\text{C}] \\ T_{c,\text{out}} \in [-20^\circ\text{C}, 120^\circ\text{C}] \\ T_{r,\text{out}} \in [5^\circ\text{C}, 60^\circ\text{C}] \\ \text{SoC} \in [30\%, 80\%] \end{cases} \quad (16)$$

The constraints (15) on the controlled inputs simply ensure that their domain of definition is enforced (e.g., pumps can either be on or off, and the resistor cannot exert a negative power, or provide more than 100% of its power). Indeed, for u_c , u_r and u_{grid} , these constraints are implicit in their definition as binary variables. The state constraints (16) ensure, on one hand, that the temperatures in the different compartments of the system allow smooth operation of the plant, avoid damaging the components, and ensure safety for the potential occupants. On the other hand, (16) imposes that the state of charge is kept in the interval in which the battery pack does not get damaged. All of these bounds are constant, apart from the lower ($T_{lb,k}$) and upper ($T_{ub,k}$) bounds on T_{room} , which are function of the time instant k . More precisely,

$$\begin{cases} T_{lb,k} = 20^\circ\text{C}, T_{ub,k} = 22^\circ\text{C} & \text{between 7 a.m. and 10 p.m.} \\ T_{lb,k} = 18^\circ\text{C}, T_{ub,k} = 20^\circ\text{C} & \text{between 10 p.m. and 7 a.m.} \end{cases} \quad (17)$$

Finally, the cost function to be minimized is related to the overall electricity cost $J_{t,n}$ defined in (7). More precisely, given an initial state at time k , a sequence of input variables

$$\mathbf{u} = \{u_0 \ u_1 \ \dots \ u_{N-1}\} \quad (18)$$

over a *prediction horizon* of N sampling intervals, and the values of the external inputs such as T_{amb} , E_e , and q_e over the same prediction horizon, one can determine a value for $J_{t,n}$ with $\tilde{N} = N$, with the difference that here we refer to a *predicted* behavior, rather than a measured one.

The MPC control law runs as follows: at each sampling time, the four temperatures are measured by the PT1000 RTD and NTC10K sensors, while the state of charge is obtained from the charge controller Power Tarom Steca 2070SC. An open-loop optimal control problem is thus solved for the given model, constraints, cost function, and measured initial state, determining the optimal sequence of future control moves

$$\mathbf{u}^* = \{u_0^* \ u_1^* \ \dots \ u_{N-1}^*\}. \quad (19)$$

These are not all applied to the process: indeed, only the first sample $u(k) = u_0^*$ is actually applied, and the remaining moves are discarded. After one sampling time, a new optimal control problem based on new measurements is solved over a shifted prediction horizon. This way of operating, known as “receding horizon”, makes MPC a closed-loop control strategy.

The future evolution of the state in (14) depends on the evolution of d along the prediction horizon, which in turn depends on future weather conditions. Therefore, weather forecast data have been used in real time, obtaining estimates of d referred to as $\hat{d} = [\hat{E}_e \ \hat{T}_{\text{amb}}]^T$.

The forecast of \hat{d} is obtained in this work by combining (in real time) weather forecast data from two different web sources² together with the values measured by the weather station. While

²Data are downloaded at each sampling instant from <http://meteocenter.asia/?m=aopa&p=35188> and http://www.yr.no/place/Kazakhstan/Astana/Astana/hour_by_hour_detailed.html.

the forecast of \hat{T}_{amb} is directly provided, the web sources do not provide \hat{E}_e , but only the so-called *cloud cover*, which in short represents the percentage of sky covered by clouds in a specific area. The estimate of the future solar irradiance is generated as $\hat{E}_e = c_{cf} \hat{E}_{ecs}$, where c_{cf} is the *cloud coefficient*, and \hat{E}_{ecs} is the value of solar irradiance under the *clear-sky* assumption. Future values of \hat{E}_{ecs} are generated for the given day, time and specific geographic coordinates, depending on several variables (including the air mass, the height of the sun above the horizon, the geographical latitude of the area, the angle of declination of the sun, and the albedo) using a freely available software [29] based, among others, on the simplified model proposed in [30]. Regarding c_{cf} , relying on data measured in the period 2012-2014, a polynomial function was obtained to provide its estimate based on the cloud cover. Based on this procedure, it was possible to obtain a prediction of \hat{d} to be used by MPC.

The optimal control problem to be solved at every sampling instant can be expressed as

$$\min_{\mathbf{u}} \sum_{k=0}^{N-1} \beta P_{\text{tot},k} \cdot q_{e,k} \cdot u_{\text{grid},k} \quad (20a)$$

$$\text{s.t.} \begin{cases} x_0 = x(k) \\ x_{k+1} = f(x_k, u_k, \hat{d}_k), k = 0, \dots, N-1 \\ u_k \in \mathcal{U}, k = 0, \dots, N-1 \\ x_k \in \mathcal{X}_k, k = 1, \dots, N \end{cases} \quad (20b)$$

The first two lines in (20b) are equality constraints which enforce the system dynamics along the prediction horizon, while the other lines are inequality (operational) constraints. Following a common practice in MPC applications, the state constraints defined by set \mathcal{X}_k are not enforced as *hard constraints*, but rather as *soft constraints*: a penalty term is added in the cost function (20a) to penalize their violation. Thus, if no feasible solution is found for which all constraints are satisfied, the MPC controller will determine the sequence that minimizes the amount of violation of the state constraints. This approach avoids the risk of not having any feasible solution available during plant operation. In the results shown in Section 4, the prediction horizon has been set as $N = 36$, which corresponds to 12 hours. The optimization algorithm is *warm-started*: the optimal control sequence \mathbf{u}^* determined at the previous sampling instant is employed to provide an initial guess for the MILP that is currently being solved. The optimal control problem defined in (20) is formulated with the Hybrid Toolbox [31] by expressing the system dynamics in MLD form, using the description language HYSDEL [32]. The resulting MILP is solved using the solver of the Gurobi Optimizer on the control computer, which is a Toshiba Satellite mM840, with Processor Intel Core i5, 4GB RAM running Windows 7. The data from sensors and weather forecast are acquired by MATLAB R2013a via ad-hoc interfaces. A data acquisition device NI DAQ 784 manages the communication with the pumps and the temperature sensors, while all other devices are directly interfaced with the control computer. The overall communication scheme is shown in Fig. 3.

4. Experimental results

The proposed MPC control law was first tested in simulation on the nominal model of the smart house, using real data for the time evolution of the disturbance vector d . Preliminary simulation results were presented in [26], in which u_{res} was a binary signal, and the actual future evolution of d was used instead of the forecast in the MPC problem. In this work, the control system is tested on the actual experimental site, which also implies the use of weather forecast. Also, considering the fact that the smart house was built internally to Nazarbayev University for research purposes rather than being a turnkey plant provided by an external company, the constant physical presence of an operator was required for guaranteeing the safety of the equipment in case of malfunctioning. Therefore, the control system could not be kept in operation for very long periods. Considering the fact that the smart house is only equipped for heating and not for cooling, the experiments need to be conducted when the ambient temperature never exceeds the imposed values of the room temperature (i.e., about 20°C), which for the city of Astana translates roughly to mid-September to mid-April. In the following, the results for a period of approximately two days (precisely, 47 hours), recorded from 12:53 a.m. on 31 March 2016, are presented.

Fig. 4 shows the evolution of the external inputs measured from the weather station: one can notice that the first day was sunnier and slightly colder than the second. Fig. 5 shows the time evolution of the state variables. The value of T_{room} is always kept within the given boundaries during daytime, while it slightly violates the upper boundary at night time. The slight violation of the bound can be caused by model inaccuracies, while the decision of keeping T_{room} close to its upper bound at night is probably due to the availability of charge in the battery, also shown in Fig. 5. The value of SoC (provided by the charge controller with a quantization of 8%, which adds another difficulty for the MPC controller) always satisfies the constraints introduced in (16). Finally, in Fig. 5 it is shown that the other temperatures ($T_{\text{c,out}}$, $T_{\text{r,out}}$ and T_{w}) are also kept within the boundaries defined in (16). In particular, T_{w} is often kept right below its upper bound of 80°C. Fig. 6 shows the control signals. The collector pump (u_c) is typically switched off in the morning, when the solar collectors have not received enough solar irradiance and $T_{\text{c,out}}$ is low: this avoids heat transfer outside the house. Notice that the values reported for u_{res} represent the percentage ([0,1]) of time during the 20 minutes sampling interval in which the resistor is on, as resulting from the implemented duty cycle. In general, the pattern of the control variables is difficult to be interpreted a posteriori, since it depends in a non-intuitive way on the solution of (20). For this specific case, however, the evolution of u_{grid} can be easily interpreted: due to a relatively mild weather, the battery can easily power the load while being charged, which allows it to provide energy at night as well. As a consequence, the MPC controller tends not to use the grid, to minimize costs (the energy from the battery has zero cost). However, after about 45 hours and with a relatively low value of SoC, the controller decides to draw energy from the grid: this is probably due to a predicted viola-

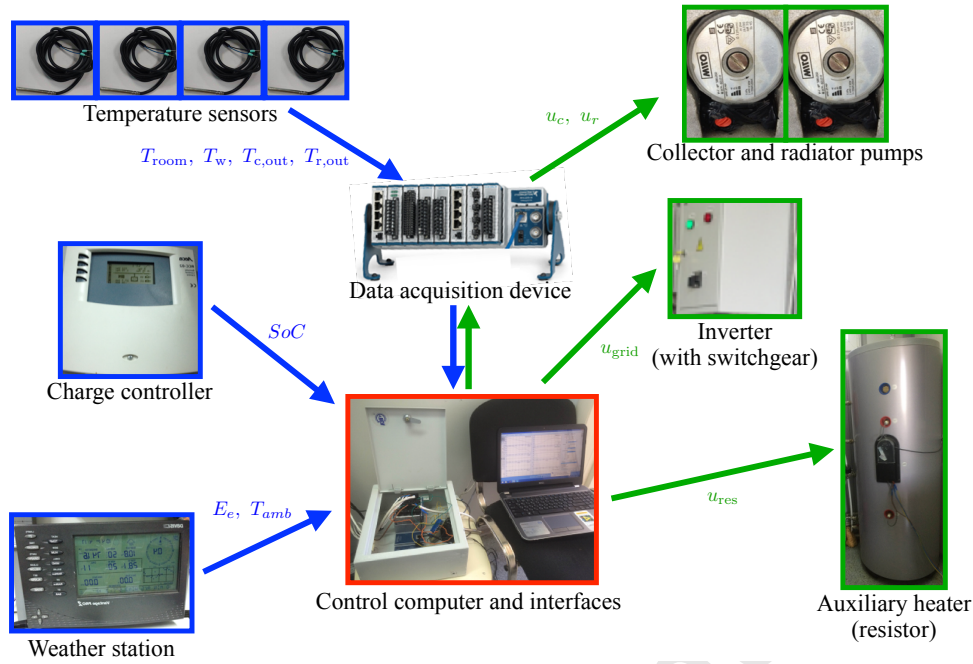


Figure 3: Communication scheme of the smart house. The data flows of sensors and actuators are represented in blue and green, respectively.

tion of the lower bound on SoC in case the battery were used. In case of colder days, the controller would instead impose frequent changes in the value of u_{grid} , as shown in the simulations in [26].

The distribution of the computation times needed to solve (20) is shown in the histogram in Fig. 7. The solution is never provided in less than 7.5 s, and in about 68% of the cases is provided in a time interval between 7.5 s and 15 s. Higher values of the computation time probably correspond to cases in which the previous solution provided for the warm start needs to be heavily modified, due to a discrepancy between the actual and predicted values of the states, or to a change in the weather forecast. The computation time is capped at 120 s (i.e., 10% of T_s): if no optimal solution is provided at this point, the current sub-optimal solution is used to determine the value of u (this only happened in 6 cases out of 140).

5. Conclusions and outlook

This paper has introduced a hybrid MPC scheme based on MILP to optimally manage, in a centralized way, the electrical and thermal subsystems of a prototype smart house. The experimental results show that the proposed control scheme achieves the required performance (i.e., it avoids large constraint violations while aiming to minimize the expense for the consumer). The battery state of charge SoC was directly obtained from the available charge controller: the resulting quantization on the SoC value has certainly caused a slight degradation of the MPC performance as compared to having a non-quantized SoC estimate. Future work will be devoted to designing a state-of-charge estimator to overcome this limitation. Another objective of future work will be to run simulations over longer pe-

riods, in order to be able to better evaluate the performance of the proposed solution. Finally, one can observe that the computation effort for solving the MILP, although acceptable for a proof of concept, would not be justified in a realistic implementation. Therefore, future effort will be put in finding reliable low-complexity approximations of the proposed hybrid MPC law, that can lower the computation time, while still providing an acceptable performance.

Acknowledgements

This research was funded under the target program 0115PK03041 “Research and development in the fields of energy efficiency and energy saving, renewable energy sources and environmental protection for years 2014-2016” from the Ministry of Education and Science of the Republic of Kazakhstan, under project n. 8 (Integration, Automation and Control of Renewable Power Sources).

References

- [1] A. I. Dounis, C. Caraiscos, Advanced control systems engineering for energy and comfort management in a building environment: A review, *Renew. Sust. Energ. Rev.* 13 (6) (2009) 1246–1261.
- [2] M. Killian, M. Kozek, Ten questions concerning model predictive control for energy efficient buildings, *Building and Environment* 105 (2016) 403–412.
- [3] S. Prívvara, J. Široký, L. Ferkl, J. Cigler, Model predictive control of a building heating system: The first experience, *Energ. Buildings* 43 (2) (2011) 564–572.
- [4] J. Široký, F. Oldewurtel, J. Cigler, S. Prívvara, Experimental analysis of model predictive control for an energy efficient building heating system, *Appl. Energy* 88 (9) (2011) 3079–3087.

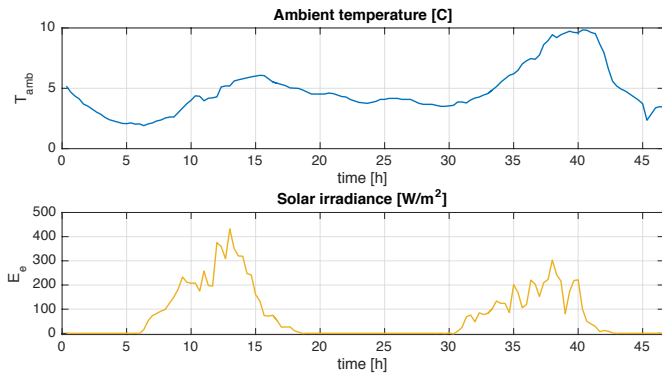


Figure 4: Time evolution of the disturbances during experimental validation, from top to bottom, respectively: T_{amb} and E_e .

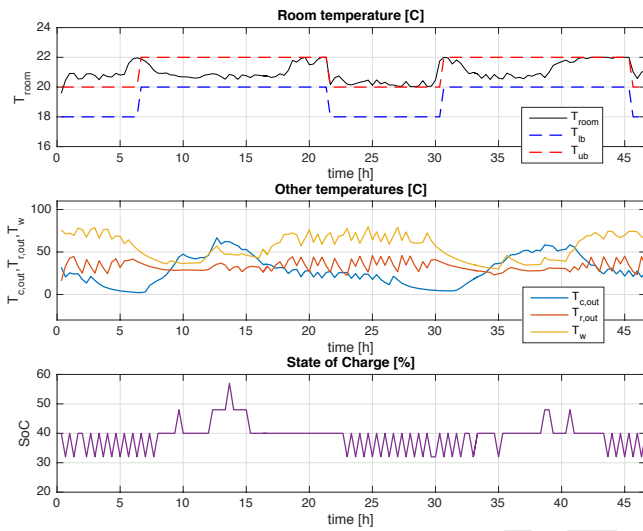


Figure 5: Time evolution of the state variables during experimental validation, from top to bottom, respectively: T_{room} with its time-varying upper and lower bounds; $T_{c,out}$, $T_{r,out}$ and T_w ; the battery state of charge SoC.

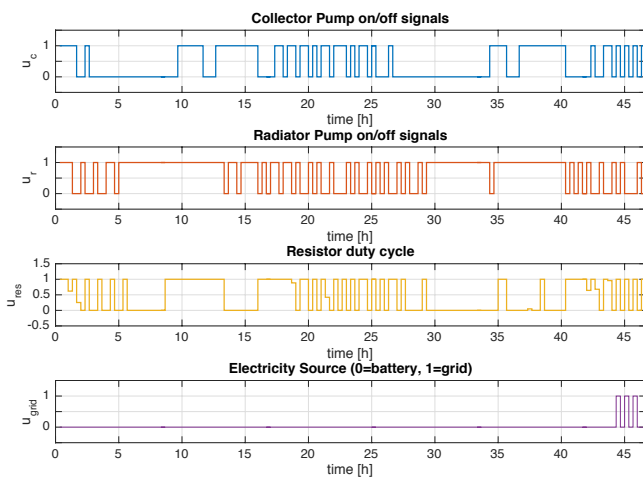


Figure 6: Time evolution of the control variables during experimental validation, from top to bottom, respectively: u_c , u_r , u_{res} , u_{grid} .

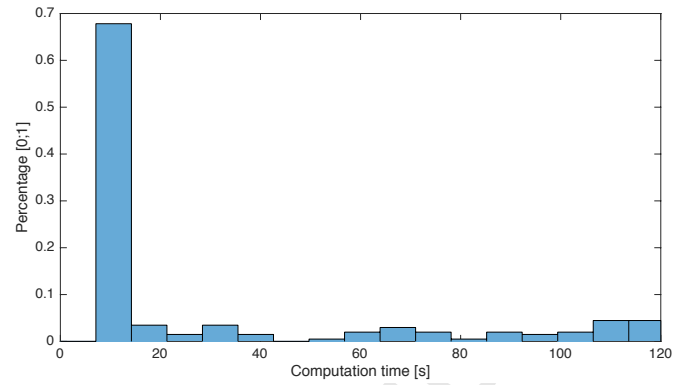


Figure 7: Histogram representing the distribution of the MILP computation time for the shown experimental results.

- [5] T. Ferhatbegović, P. Palensky, G. Fontanella, D. Basciotti, Modelling and design of a linear predictive controller for a solar powered HVAC system, in: IEEE Int. Symp. on Ind. Electron., 2012, pp. 869–874.
- [6] Y. Ma, F. Borrelli, B. Hancey, B. Coffey, S. Bengea, P. Haves, Model predictive control for the operation of building cooling systems, IEEE Trans. Contr. Sys. Tech. 20 (3) (2012) 796–803.
- [7] S. J. Kang, J. Park, K.-Y. Oh, J. G. Noh, H. Park, Scheduling-based real time energy flow control strategy for building energy management system, Energ. Buildings 75 (2014) 239–248.
- [8] S. C. Bengea, A. D. Kelman, F. Borrelli, R. Taylor, S. Narayanan, Implementation of model predictive control for an HVAC system in a mid-size commercial building, HVAC&R Res. 20 (1) (2014) 121–135.
- [9] R. De Coninck, L. Helsen, Practical implementation and evaluation of model predictive control for an office building in Brussels, Energy and Buildings 111 (2016) 290–298.
- [10] F. Oldewurtel, A. Parisio, C. N. Jones, D. Gyalistras, M. Gwerder, V. Stauch, B. Lehmann, M. Morari, Use of model predictive control and weather forecasts for energy efficient building climate control, Energ. Buildings 45 (2012) 15–27.
- [11] F. Oldewurtel, C. N. Jones, A. Parisio, M. Morari, Stochastic model predictive control for building climate control, IEEE Trans. Contr. Sys. Tech. 22 (3) (2014) 1198–1205.
- [12] Y. Ma, J. Matusko, F. Borrelli, Stochastic model predictive control for building HVAC systems: Complexity and conservatism, IEEE Trans. Contr. Sys. Tech. 23 (1) (2015) 101–116.
- [13] R. R. Neegenborn, M. Houwing, B. De Schutter, J. Hellendoorn, Model predictive control for residential energy resources using a mixed-logical dynamic model, in: Int. Conf. on Networking, Sensing and Control, 2009, pp. 702–707.
- [14] F. Berkenkamp, M. Gwerder, Hybrid model predictive control of stratified thermal storages in buildings, Energ. Buildings 84 (2014) 233–240.
- [15] J. D. Feng, F. Chuang, F. Borrelli, F. Bauman, Model predictive control of radiant slab systems with evaporative cooling sources, Energ. Buildings 87 (2015) 199–210.
- [16] E. Herrera, R. Bourdais, H. Guéguen, A hybrid predictive control approach for the management of an energy production–consumption system applied to a TRNSYS solar absorption cooling system for thermal comfort in buildings, Energ. Buildings 104 (2015) 47–56.
- [17] H. Huang, L. Chen, E. Hu, A hybrid model predictive control scheme for energy and cost savings in commercial buildings: simulation and experiment, in: American Control Conference, 2015, pp. 256–261.
- [18] H. T. Nguyen, D. T. Nguyen, L. B. Le, Energy management for households with solar assisted thermal load considering renewable energy and price uncertainty, IEEE Trans. on Smart Grid 6 (1) (2015) 301–314.
- [19] H. Borhan, A. Vahidi, A. M. Phillips, M. L. Kuang, I. V. Kolmanovskiy, S. Di Cairano, MPC-based energy management of a power-split hybrid electric vehicle, IEEE Trans. Contr. Sys. Tech. 20 (3) (2012) 593–603.
- [20] S. Di Cairano, D. Bernardini, A. Bemporad, I. V. Kolmanovskiy, Stochastic MPC with learning for driver-predictive vehicle control and its application to HEV energy management, IEEE Trans. Contr. Sys. Tech. 22 (3)

- (2014) 1018–1031.
- [21] A. Lefort, R. Bourdais, G. Ansanay-Alex, H. Guéguen, Hierarchical control method applied to energy management of a residential house, *Energ. Buildings* 64 (2013) 53–61.
 - [22] H. Dagdougui, R. Minciardi, A. Ouammi, M. Robba, R. Sacile, Modeling and optimization of a hybrid system for the energy supply of a “green” building, *Energy Conversion and Management* 64 (2012) 351–363.
 - [23] C. Chen, J. Wang, Y. Heo, S. Kishore, MPC-based appliance scheduling for residential building energy management controller, *IEEE Transactions on Smart Grid* 4 (3) (2013) 1401–1410.
 - [24] X. Li, J. Wen, Review of building energy modeling for control and operation, *Renewable and Sustainable Energy Reviews* 37 (2014) 517–537.
 - [25] A. Bemporad, M. Morari, Control of systems integrating logic, dynamics, and constraints, *Automatica* 35 (3) (1999) 407–427.
 - [26] A. Khakimova, A. Shamshimova, D. Sharipova, A. Kusatayeva, V. Ten, A. Bemporad, Y. Familiant, A. Shintemirov, M. Rubagotti, Hybrid model predictive control for optimal energy management of a smart house, in: *IEEE 15th International Conference on Environment and Electrical Engineering*, 2015, pp. 513–518.
 - [27] Solar module series alfasolar Pyramid 60P - Datasheet, http://en.alfasolar.biz/uploads/media/alfasolar-pyramid-60P-ENG-052014_small_01.pdf (2014).
 - [28] L. Ljung, *System identification: Theory for the user*, Springer, 1998.
 - [29] A solar position and radiation calculator for Microsoft Excel/VBA, <http://www.ecy.wa.gov/programs/eap/models/solrad.zip>, accessed: 2016-08-23.
 - [30] R. E. Bird, R. L. Hulstrom, Simplified clear sky model for direct and diffuse insolation on horizontal surfaces, Tech. rep., Solar Energy Research Inst., Golden, CO (USA) (1981).
 - [31] A. Bemporad, Hybrid Toolbox - User’s Guide, <http://cse.lab.imtlucca.it/~bemporad/hybrid/toolbox> (2004).
 - [32] F. Torrisi, A. Bemporad, HYSDEL — A tool for generating computational hybrid models, *IEEE Trans. Contr. Systems Technology* 12 (2) (2004) 235–249.